Constraints on the threshold K^- nuclear potential from FINUDA ${}^A\mathrm{Z}(K^-_{\mathrm{stop}},\pi^-){}^A_\Lambda\mathrm{Z}$ spectra

A. Cieplý[a], E. Friedman[b], A. Gal[b,*], V. Krejčiřík[a,c]

[a] *Nuclear Physics Institute, 25068 Řež, Czech Republic*
[b] *Racah Institute of Physics, The Hebrew University, 91904 Jerusalem, Israel*
[c] *Department of Physics, University of Maryland, College Park, MD 20742-4111, USA*

Abstract

$1s_\Lambda$ hypernuclear formation rates in stopped K^- reactions on several p-shell targets are derived from hypernuclear formation spectra measured recently by the FINUDA Collaboration and are compared with calculated $1s_\Lambda$ formation rates based on a $\bar{K}N$ coupled channels chiral model. The calculated rates are about 15% of the derived rates, and in contrast with previous calculations depend weakly on the depth of the threshold K^- nuclear potential. The A dependence of the calculated $1s_\Lambda$ rates is in fair agreement with that of the derived $1s_\Lambda$ rates, showing a slight preference for a deep density dependent potential, $\mathrm{Re}\,V_{K^-}(\rho_0) \sim -(150\text{–}200)$ MeV, over a shallow potential, $\mathrm{Re}\,V_{K^-}(\rho_0) \sim -50$ MeV. These new features originate from a substantial energy and density dependence found for the subthreshold $K^-n \to \pi^-\Lambda$ branching ratio that serves as input to the K^- capture at rest calculations.

Keywords: hypernuclei, kaon-induced reactions, mesonic atoms
PACS: 21.80.+a, 25.80.Nv, 36.10.Gv

1. Introduction

How strong is the K^- nuclear interaction? Various scenarios proposed for kaon condensation in dense neutron-star matter [1], and more recently for quasibound K^- nuclear clusters [2] and for self-bound strange hadronic matter [3] depend on the answer to this question which has not been resolved todate. A modern theoretical framework for the underlying low-energy $\bar{K}N$

*Corresponding author: Avraham Gal, avragal@vms.huji.ac.il

interaction is provided by the leading-order Tomozawa-Weinberg vector term of the chiral effective Lagrangian which, in Born approximation, yields a sizable attraction for the K^- nuclear potential V_{K^-}:

$$V_{K^-} = -\frac{3}{8f_\pi^2}\,\rho \sim -57\,\frac{\rho}{\rho_0}\ \ \text{(in MeV)} \tag{1}$$

for $\rho_0 = 0.17$ fm^{-3}, where $f_\pi \sim 93$ MeV is the pseudoscalar meson decay constant. This attraction is doubled, roughly, within a unitarized coupled-channel $\bar{K}N - \pi\Sigma - \pi\Lambda$ calculation which provides also for a strong absorptivity [4]. Shallower potentials, with Re $V_{K^-}(\rho_0) \sim -(40\text{–}60)$ MeV, are obtained by imposing a Watson-like self-consistency requirement on the nuclear-medium K^-N $t(\rho)$ matrix that enters the optical potential $V_{K^-} = t(\rho)\rho$ [5, 6]. In contrast, comprehensive global fits to K^--atom strong-interaction shifts and widths yield extremely deep density dependent optical potentials at threshold, in the range Re $V_{K^-}(\rho_0) \sim -(150\text{–}200)$ MeV [7]. In this Letter we discuss recent FINUDA measurements that might bear on this issue by providing constraints on the strength of the threshold K^- nuclear attraction.

In the preceding Letter [8], the FINUDA Collaboration at DAΦNE, Frascati, reported on Λ-hypernuclear spectra taken in the $K^-_{\rm stop} + {}^A{\rm Z} \to \pi^- + {}^A_\Lambda{\rm Z}$ reaction on several p-shell nuclear targets. Formation rates were given per stopped K^- for bound states and for low lying continuum states. In ${}^{16}_\Lambda$O the bound state formation rates agree nicely with a previous KEK measurement [9]. The recent FINUDA data allow for the first time to consider the A dependence of the formation rates in detail within the nuclear p shell where nuclear structure effects may be reliably separated out. It is our purpose in this companion Letter to apply one's knowledge of the nuclear structure aspect of the problem in order to extract the dynamical contents of the measured formation rates, particularly that part which concerns the K^- nuclear dynamics at threshold. In doing so we transform the partial formation rates reported for well defined and spectroscopically reliable final Λ hypernuclear states into $1s_\Lambda$ hypernuclear formation rates that allow direct comparison with DWIA calculations.

The expression for the formation rate of hypernuclear final state f in capture at rest on target g.s. i, apart from kinematical factors, is a product of two dynamical factors [10, 11, 12]: (i) the branching ratio for $K^-n \to \pi^-\Lambda$ in K^- absorption at rest in the nuclear medium, here denoted BR; and (ii)

the absolute value squared of a DWIA amplitude given by

$$T_{fi}^{\rm DWIA}(\mathbf{q}_f) = \int \chi^{(-)*}_{\mathbf{q}_f}(\mathbf{r})\, \rho_{fi}(\mathbf{r})\, \Psi_{nLM}(\mathbf{r})\, d^3r, \tag{2}$$

divided for a proper normalization by the integral $\overline{\rho}$ of the K^- atomic density overlap with the nuclear density $\rho(r)$

$$\overline{\rho} = \int \rho(r) \mid \Psi_{nLM}(\mathbf{r}) \mid^2 \; d^3r. \tag{3}$$

Here ρ_{fi} stands for the nuclear to hypernuclear transition form factor, $\chi^{(-)}_{\mathbf{q}_f}$ is an outgoing pion distorted wave generated by a pion optical potential fitted to scattering data, and Ψ_{nLM} is a K^- atomic wavefunction obtained by solving the Klein-Gordon equation with a K^- nuclear strong interaction potential V_{K^-} added to the appropriate Coulomb potential. The integration on the r.h.s. of Eq. (2) is confined by the bound-state form factor ρ_{fi} to within the nucleus, where Ψ_{nLM} is primarily determined by the strong-interaction V_{K^-}, although Ψ_{nLM} is an atomic wavefunction that peaks far outside the nucleus. The sensitivity of the DWIA amplitude Eq. (2) to V_{K^-} is owing to the interference of Ψ_{nLM} with the oscillatory pion distorted wave $\chi^{(-)}_{\mathbf{q}_f}$. Assuming that ρ_{fi} and $\chi^{(-)}_{\mathbf{q}_f}$ are under fair phenomenological control, it is the initial-state dynamical contents due to Ψ_{nLM} that is tested by studying the $1s_\Lambda$ formation rates in K^- capture at rest, as verified in past DWIA calculations [10, 11, 12]. While this holds true, we point out in this Letter another strong sensitivity to the initial-state K^- nuclear dynamics arising from the energy and density dependence of the $K^-n \to \pi^-\Lambda$ BR. Here we show how to incorporate this energy and density dependence into the calculation of a properly averaged value $\overline{\rm BR}$ which depends on the K^- atomic orbit through L and on the mass number A of the target. The resulting calculated $1s_\Lambda$ formation rates are then compared to those derived from the FINUDA data and conclusions are made on the deep vs. shallow K^- nuclear potential issue.

2. Derivation of $1s_\Lambda$ capture rates from FINUDA data

The FINUDA spectra show distinct peaks for several $1s_\Lambda$ and $1p_\Lambda$ states in the nuclear p shell. In general, the derivation of the $1p_\Lambda$ formation rate is ambiguous given that the $1p_\Lambda$ formation strength is often obscured by a rising Λ continuum. In ${}^{9}_{\Lambda}$Be and in ${}^{13}_{\Lambda}$C it is also mixed with a substantial part of the

$1s_\Lambda$ formation strength owing particularly to high lying $T = 1$ parent states in the corresponding core nuclei. For this reason, we here deal only with the $1s_\Lambda$ formation strength, attempting to derive it from an unambiguous identification of *low lying* $1s_\Lambda$ hypernuclear states. For such states we use the theoretical framework of Ref. [13] in which hypernuclear formation rates are expressed in terms of a $1s_\Lambda$ formation rate, which is independent of the particular hypernuclear state, times a structure fraction which is derived from neutron pick-up spectroscopic factors in the target nucleus. This theoretical framework is also applicable to forward cross sections of in-flight reactions such as (π^+, K^+) and $(e, e'K^+)$. In Table 1 we present $1s_\Lambda$ formation rates derived from the FINUDA K^- capture at rest hypernuclear spectra [8, 14] for a procedure denoted (a). In each spectrum we focus on the strongest low-lying particle-stable hypernuclear excitation which is also well described in terms of a Λ hyperon weakly coupled to a nuclear core parent state. These core parent states are specified in the table. The measured formation rates are then divided by the corresponding structure fractions to obtain $1s_\Lambda$ formation rates. For comparison, we display in the last column the $1s_\Lambda$ component of forward-angle integrated (π^+, K^+) cross sections (KEK-E336 [16]) derived using the peaks listed in the second and third columns. These (π^+, K^+) strengths show little A dependence, in contrast to the K^- capture at rest $1s_\Lambda$ formation rates that decrease by a factor 3.5 in going from ^{7}Li to ^{16}O.

Table 1: $1s_\Lambda$ formation rates $R(1s_\Lambda)$ per stopped K^-, derived from the strongest hypernuclear bound state peak for each of the listed targets [procedure (a)]. Data are taken from the preceding Letter [8], and for $^{12}_{\Lambda}$C from [14]. The errors are statistical and systematic, in this order. The $1s_\Lambda$ structure fractions are from [15] and, if unlisted there, from [13]. Listed in the last column, for comparison, are $1s_\Lambda$ forward-angle integrated (π^+, K^+) cross sections, derived also by using procedure (a) from KEK-E336 measurements [16].

target ^{A}Z	peak $J^\pi_{\rm core}$	$E^*_{\rm core}$ (MeV)	$1s_\Lambda$ frac.	$R(1s_\Lambda) \times 10^3$ per stopped K^-	$\sigma_{1s_\Lambda}(\mu b)$ (π^+, K^+)
^{7}Li	3^+	2.19	0.311	$1.48 \pm 0.16 \pm 0.19$	1.56 ± 0.10
^{9}Be	2^+	2.94	0.242	$0.87 \pm 0.08 \pm 0.12$	1.40 ± 0.05
^{12}C	$(3/2)^-$	g.s.	0.810	$1.25 \pm 0.14 \pm 0.12$	1.78 ± 0.04
^{13}C	2^+	4.44	0.224	$0.85 \pm 0.09 \pm 0.13$	1.87 ± 0.09
^{16}O	$(3/2)^-$	6.18	0.618	$0.42 \pm 0.06 \pm 0.06$	1.47 ± 0.05

In the second procedure, denoted (b) and presented in Table 2, we consider all the particle-stable $1s_\Lambda$ states corresponding to observed peaks for

which the shell model offers reliable identification. For three of the five targets listed, this procedure saturates or is close to saturating the $1s_\Lambda$ formation strength. However, in both ${}^{9}_{\Lambda}$Be and ${}^{13}_{\Lambda}$C the $1s_\Lambda$ particle stable hypernuclear states represent less than half of the full $1s_\Lambda$ strength. In passing we remark that in ${}^{13}_{\Lambda}$C we have ignored the third peak at 7.6 MeV excitation, apparently based on the 0^+ 'Hoyle state' in ^{12}C, because the shell model fails to explain it in natural terms. Similarly to Table 1, in the last column of Table 2 we assembled $1s_\Lambda$ forward-angle integrated (π^+, K^+) cross sections, derived from KEK-E336 measurements [16] by applying procedure (b). Here too, the weak A dependence of these $1s_\Lambda$ (π^+, K^+) cross sections is in stark contrast to the fast decrease of the $1s_\Lambda$ formation rates, again by a factor 3.5, going from ^{7}Li to ^{16}O in K^- capture at rest. The strong A dependence of the $(K^-_{\rm stop}, \pi^-)$ rates with respect to the weak A dependence of the (π^+, K^+) cross sections reflects the sizable difference between the strongly attractive K^- nuclear interaction at threshold and the weakly repulsive K^+ nuclear interaction.

Table 2: Same as in Table 1 except for using several (rather than one) well defined $1s_\Lambda$ bound states for each of the listed targets [procedure (b)].

target ^{A}Z	peaks	$1s_\Lambda$ frac.	$R(1s_\Lambda) \times 10^3$ per stopped K^-	$\sigma_{1s_\Lambda}(\mu b)$ (π^+, K^+)
^{7}Li	1,2,3	0.833	$1.25 \pm 0.14 \pm 0.17$	1.29 ± 0.12
^{9}Be	1,2	0.435	$0.85 \pm 0.09 \pm 0.11$	1.20 ± 0.05
^{12}C	1,2,3	0.995	$1.67 \pm 0.23 \pm 0.23$	1.92 ± 0.07
^{13}C	1,2	0.347	$0.84 \pm 0.12 \pm 0.12$	1.93 ± 0.12
^{16}O	1,2	1.000	$0.36 \pm 0.06 \pm 0.05$	1.32 ± 0.05

Comparing the two procedures (a) and (b) in Tables 1 and 2, respectively, it is encouraging to see that within statistical uncertainties both sets of $R(1s_\Lambda)$ values are consistent with each other, except marginally for ^{12}C which dates back to a separate FINUDA run [14]. Procedure (a) yields a value for ^{12}C that compares well with $R(1s_\Lambda)[{}^{12}{\rm C}] = (1.11 \pm 0.14)\ 10^{-3}$ per stopped K^-, the latter value corresponding to $E_x \lesssim 7$ MeV in the ${}^{12}_{\Lambda}$C spectrum from KEK [9]. Therefore, in the present study we adopt the $R(1s_\Lambda)$ values listed in Table 1.

3. Energy dependent $K^-n \to \pi^-\Lambda$ branching ratios

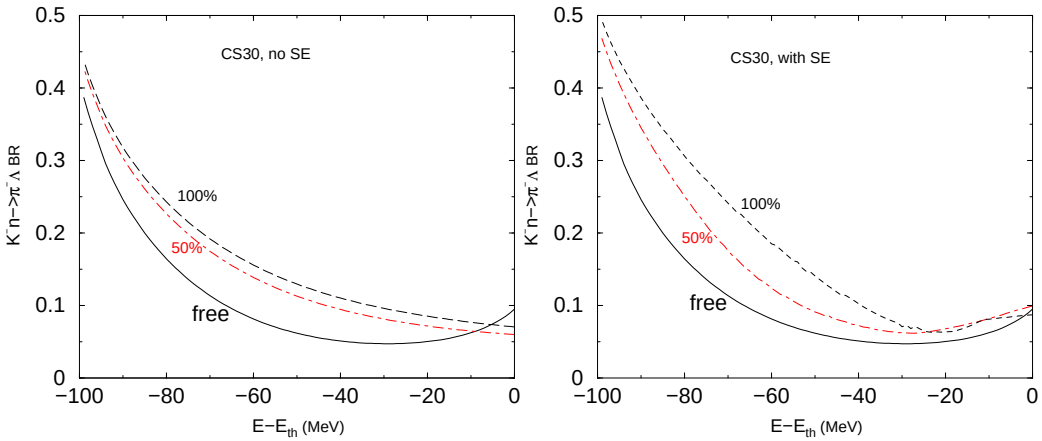

Figure 1: Subthreshold energy dependence of the $K^-n \to \pi^-\Lambda$ branching ratio BR in the CS30 version of the chiral model, Ref. [17]. The l.h.s. curves for $50, 100\%$ nuclear matter density demonstrate Pauli blocking effects whereas the r.h.s. curves account additionally for self energy effects.

Figure 1 shows the subthreshold energy dependence of the free-space $K^-n \to \pi^-\Lambda$ BR generated by the CS30 version of the coupled channel chiral model of Ref. [17].[1] This $I = 1$ BR is about 10% at threshold, decreasing to roughly half of its value as the $I = 0$ $\Lambda(1405)$ subthreshold resonance is traversed, and then increases to approximately 40% on approaching the $\pi\Sigma$ threshold about 100 MeV below the $\bar{K}N$ threshold. The figure also shows the in-medium BR below threshold at densities 50% and 100% of nuclear matter density ρ_0, in two versions of medium modifications. In the l.h.s. plots the only medium effect is Pauli blocking, which acts in intermediate $\bar{K}N$ states in the coupled channel equations. This is known to have the effect of pushing the dynamically generated $\Lambda(1405)$ to energies above threshold [18, 19], thus weakening the $I = 0$ interaction and consequently increasing the $I = 1$ BR. The energy dependence in the subthreshold region is seen to be monotonic. The r.h.s. plots include in addition to Pauli blocking also meson and baryon self-energy (SE) terms in intermediate state propagators. This

[1] The parameters of CS30 are constrained by $\sigma_{\pi N} = 30$ MeV.

pushes back the $\Lambda(1405)$ [5, 20] and in the chiral model used here [17] results in stronger energy and density dependencies. The same chiral model was used in Ref. [12] to generate a $K^-n \to \pi^-\Lambda$ BR which, however, was fixed at its threshold value, thus neglecting any possible energy dependence. Since the in-medium BRs plotted in Fig. 1 exhibit a sizable energy and density dependence, it is essential to consider the implied effects in the evaluation of the $1s_\Lambda$ formation rates.

In the chiral model of Ref. [17] the $K^-n \to \pi^-\Lambda$ BR depends on the initial K^-n invariant energy $\sqrt{s}$, with $s = (E_K + E_N)^2 - (\vec{p}_K + \vec{p}_N)^2$ in obvious notation. In the two-body c.m. system $\vec{p}_K + \vec{p}_N = 0$, but in the K^-–nucleus c.m. system (approximately nuclear lab system) $\vec{p}_K + \vec{p}_N \neq 0$ and averaging over angles yields $(\vec{p}_K + \vec{p}_N)^2 \to (p_K^2 + p_N^2)$. For bound hadrons, with $E_K = m_K - B_K$, $E_N = m_N - B_N$, we expand near threshold, $E_{\rm th} = m_K + m_N$, neglecting quadratic terms in the binding energies B_K, B_N:

$$\sqrt{s} \approx E_{\rm th} - B_N - B_K - \frac{m_N}{m_N + m_K}\,\frac{p_N^2}{2m_N} - \frac{m_K}{m_N + m_K}\,\frac{p_K^2}{2m_K}. \qquad (4)$$

For K^- capture at rest, we further neglect the atomic B_K with respect to B_N and replace the K^- kinetic energy $p_K^2/(2m_K)$ in the local density approximation by $-{\rm Re}\,V_{K^-}(\rho)$ which dominates over the K^- Coulomb potential within the range of densities of interest. The neutron kinetic energy $p_N^2/(2m_N)$ is approximated in the Fermi gas model by $23\,(\rho/\rho_0)^{2/3}$ MeV. Altogether the energy argument of the $K^-n \to \pi^-\Lambda$ BR assumes the form[2]

$$\sqrt{s} \approx E_{\rm th} - B_N - 15.1\,(\rho/\rho_0)^{2/3} + 0.345\,{\rm Re}\,V_{K^-}(\rho)\ \ ({\rm in\ MeV}) \qquad (5)$$

which unambiguously prescribes the subthreshold two-body energy as a function of nuclear density at which ${\rm BR}(\sqrt{s},\rho)$ of Fig. 1 is to be evaluated.[3] Note that Eq. (5) leads to implicit density dependence of ${\rm BR}(\sqrt{s},\rho)$ through the invariant energy variable $\sqrt{s}$, in addition to the explicit ρ dependence. The input BRs for our $1s_\Lambda$ hypernuclear formation rates calculation were obtained by averaging this chiral-model ${\rm BR}(\sqrt{s},\rho)$, for a given $V_{K^-}(\rho)$, over the K^- nuclear density overlap $\rho(r) \mid \Psi_{nLM}(\mathbf{r}) \mid^2$ of Eq. (3):

$$\overline{\rm BR} = \frac{1}{\overline{\rho}} \int {\rm BR}(\sqrt{s},\rho)\,\rho(r) \mid \Psi_{nLM}(\mathbf{r}) \mid^2\ d^3r. \qquad (6)$$

[2]Applications of this form to kaonic atoms will be discussed elsewhere [21].

[3]Related ideas on the relevance of extrapolating to subthreshold energies in K^- capture at rest have been repeatedly made by Wycech, see Ref. [22].

For B_N we used target neutron separation energies. The nuclear densities used were obtained from MHO nuclear charge densities by unfolding the finite size of the proton. The structure of Eqs. (5), (6), together with the plots of Fig. 1, imply that deep K^- nuclear potentials lead to significantly higher values of $\overline{\rm BR}$ than the threshold value used in Ref. [12], which indeed is borne out by the present calculations.

4. Confronting data with DWIA calculations

The $1s_\Lambda$ formation rates for a shallow K^- nuclear potential $V_{K^-}^{\rm SH}$ of depth $-{\rm Re}\,V_{K^-}^{\rm SH}(\rho=\rho_0)\approx 50$ MeV and for a deep K^- nuclear potential $V_{K^-}^{\rm DD}$ of depth $-{\rm Re}\,V_{K^-}^{\rm DD}(\rho=\rho_0)\approx 190$ MeV have been recalculated with refined K^- wavefunctions and π^- distorted waves.[4] A major change here with respect to Refs. [12, 23] is the use of energy dependent BRs as outlined in Sect. 3. The resulting $\overline{\rm BR}$s for the deep K^- potential $V_{K^-}^{\rm DD}$ display considerable A dependence, with values higher than the threshold value used in Ref. [12], particularly from ^{12}C on. In contrast, the $\overline{\rm BR}$s for the shallow potential $V_{K^-}^{\rm SH}$ show little A dependence, with values lower than the threshold value. The difference between the DD and SH rates is no longer as large as was for a fixed BR [12]. For example, the calculated rates are about (15–18)% of the experimentally derived rate for ^{7}Li under procedure (a) using the best-fit pion optical potential π_e, Eqs. (19), (20) of Ref. [6], and (23–26)% of it using the pion optical potential π_b discussed in Ref. [12]. For ^{16}O, the difference between using $V_{K^-}^{\rm SH}$ and $V_{K^-}^{\rm DD}$ is larger for π_e: (13–30)%; the deeper the potential, the lower is the calculated rate, in agreement with past experience [6, 12]. The larger range of variation for ^{16}O with respect to that for ^{7}Li reflects the difference in A dependence between the formation rates for the K^- potentials tested here.

We focus now on the A dependence of the $1s_\Lambda$ formation rates. For given K^- and π^- potentials the calculated rates are scaled up by a normalization factor to achieve agreement for ^{7}Li with the $1s_\Lambda$ rate derived from the data under procedure (a) in Table 1. This is shown in Fig. 2 where the uncertainties of the experimentally derived $1s_\Lambda$ rates consist only of statistical errors that vary from one target to another. The systematic errors, on the other hand, are the same for all targets and drop out when considering A dependence within the present set of FINUDA data. The normalized calculated

[4] These potentials were denoted K_χ and $K_{\rm DD}$, respectively, in Ref. [12].

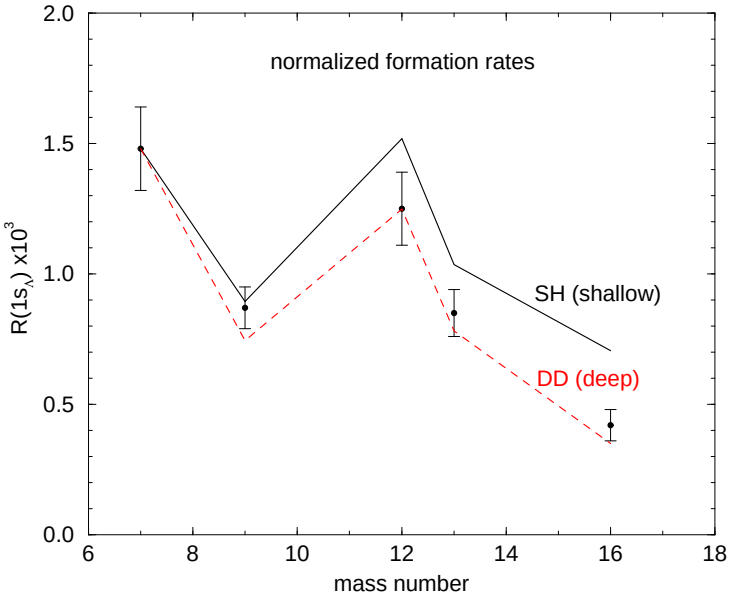

Figure 2: Comparison between $1s_\Lambda$ formation rates derived from the FINUDA K^- capture at rest data [8, 14] and DWIA calculations normalized to the $1s_\Lambda$ formation rate of ${}^{7}_{\Lambda}$Li listed in Table 1 for shallow (SH, solid) and deep (DD, dashed) K^- nuclear potentials. The calculated $1s_\Lambda$ formation rates use $K^-n \to \pi^-\Lambda$ in-medium BRs without self energies, see Sect. 3, and pion optical potential π_e from Ref. [6]. The error bars consist of statistical uncertainties only.

$1s_\Lambda$ rates shown in the figure are for the no-SE in-medium version of the chiral model CS30 [17] with $\overline{\rm BR}$s calculated according to Eq. (6). Results are shown for the pion optical potential π_e which was fitted to π^-–^{12}C angular distributions at 162 MeV [6], and for the two K^- nuclear potentials $V^{\rm SH}_{K^-}$ and $V^{\rm DD}_{K^-}$. We note that the decrease of the experimentally derived $1s_\Lambda$ rates from ^{7}Li to ^{9}Be, followed by increase for ^{12}C and subsequently decreasing through ^{13}C down to ^{16}O, is well reproduced by both calculations shown in Fig. 2. However, the deep $V^{\rm DD}_{K^-}$ calculated rates reproduce better the A dependence of the experimentally derived rates than the shallow $V^{\rm SH}_{K^-}$ potential does. Similar conclusions hold for $\overline{\rm BR}$s that are based on the SE in-medium version of CS30 plotted on the r.h.s. of Fig. 1. On the other hand, if the pion optical potential π_b (applied extensively in Ref. [12]) or π_c are used in these calculations, neither $V^{\rm DD}_{K^-}$ nor $V^{\rm SH}_{K^-}$ do as good a job as the combination $V^{\rm DD}_{K^-}$ and the best-fit π_e does, and no firm conclusion can be reached.

5. Conclusion

In conclusion, we have derived $1s_\Lambda$ hypernuclear formation rates from peak formation rates associated with the ${}^A\mathrm{Z}(K^-_{\rm stop},\pi^-){}^A_\Lambda\mathrm{Z}$ spectra presented recently by the FINUDA Collaboration on several nuclear targets in the p shell [8, 14]. We then compared the A dependence of these derived rates with that provided by calculations for the two extreme V_{K^-} scenarios discussed at present, a chirally motivated shallow potential and a density dependent deep potential. The calculations use $K^-n \to \pi^-\Lambda$ in-medium BRs generated by a chiral model. These BRs exhibit a strong subthreshold energy and density dependence, and consequently depend sensitively on the initial-state K^- nuclear potential. The calculations also demonstrate additional strong sensitivity to V_{K^-} at threshold through the atomic wavefunctions it generates and which enter into the DWIA calculation of the formation rates in stopped K^- reactions. The comparison between the calculated A dependence and that derived from the FINUDA data slightly favors a deep K^- nuclear potential over a shallow one. This conclusion outdates the one reached in an earlier version in which the energy and density dependence of the BRs, resulting here in a new source of sensitivity to V_{K^-}, was disregarded [23]. In future work, it would be interesting to extend the range of nuclear targets used in stopped K^- reactions to medium and heavy weight nuclei in order to confirm the present conclusion and to look for more subtle effects of density dependence.

Acknowledgements

We are grateful to Tullio Bressani and Germano Bonomi for useful discussions of the FINUDA measurements and to Daniel Gazda and Jiří Mareš for clarifying discussions on subthreshold extrapolations. This work was supported by the GAUK Grant No. 91509 and GACR Grant No. 202/09/1441, as well as by the EU initiative FP7, HadronPhysics2, under Project No. 227431.

References

[1] B.D. Kaplan, A.E. Nelson, Phys. Lett. B **175** (1986) 57; Phys. Lett. B **179** (1986) 409.

[2] Y. Akaishi, T. Yamazaki, Phys. Rev. C **65** (2002) 044005.

[3] D. Gazda, E. Friedman, A. Gal, J. Mareš, Phys. Rev. C **76** (2007) 055204, **77** (2008) 045206, **80** (2009) 035205.

[4] W. Weise, R. Härtle, Nucl. Phys. A **804** (2008) 173, and references therein.

[5] A. Ramos, E. Oset, Nucl. Phys. A **671** (2000) 481.

[6] A. Cieplý, E. Friedman, A. Gal, J. Mareš, Nucl. Phys. A **696** (2001) 173.

[7] E. Friedman, A. Gal, Phys. Rep. **452** (2007) 89, and references therein.

[8] M. Agnello, et al. [FINUDA Collaboration], submitted to Phys. Lett. B [arXiv:1011.2695 (nucl-ex)].

[9] H. Tamura, R.S. Hayano, H. Outa, T. Yamazaki, Prog. Theor. Phys. Suppl. **117** (1994) 1; H. Tamura, private communication (2010).

[10] A. Gal, L. Klieb, Phys. Rev. C **34** (1986) 956.

[11] A. Matsuyama, K. Yazaki, Nucl. Phys. A **477** (1988) 673.

[12] V. Krejčiřík, A. Cieplý, A. Gal, Phys. Rev. C **82** (2010) 024609.

[13] R.H. Dalitz, A. Gal, Ann. Phys. **116** (1978) 167.

[14] M. Agnello, et al. [FINUDA Collaboration], Phys. Lett. B **622** (2005) 35.

[15] D.J. Millener, A. Gal, C.B. Dover, R.H. Dalitz, Phys. Rev. C **31** (1985) 499.

[16] O. Hashimoto, H. Tamura, Prog. Part. Nucl. Phys. **57** (2006) 564.

[17] A. Cieplý, J. Smejkal, Eur. Phys. J. A **43** (2010) 191.

[18] V. Koch, Phys. Lett. B **337** (1994) 1.

[19] T. Waas, N. Kaiser, W. Weise, Phys. Lett. B **365** (1996) 12; Phys. Lett. B **379** (1996) 34.

[20] M. Lutz, Phys. Lett. B **426** (1998) 12.

[21] A. Cieplý, E. Friedman, A. Gal, D. Gazda, J. Mareš, in preparation.

[22] S. Wycech, Acta Phys. Pol. B **41** (2010) 2201, and references therein.

[23] A. Cieplý, E. Friedman, A. Gal, V. Krejčiřík, arXiv:1011.2855v1.